Electronic, Optical and Vibrational Properties of $B_3N_3H_6$ from First-Principles Calculations

Yun-Dan Gan
Xi'an Modern Chemistry Research Institute
Han Qin
Xihua University
Fu-Sheng Liu
Southwest Jiaotong University
Zheng-Tang Liu
Northwestern Polytechnical University
Cheng lu Jiang (juul@my.swjtu.edu.cn)
Southwest Jiaotong University https://orcid.org/0000-0002-2130-7760
Qi-Jun Liu
Southwest Jiaotong University

Research Article

Keywords: density functional theory, electronic structure, optical properties, B3N3H6

Posted Date: June 14th, 2021

DOI: https://doi.org/10.21203/rs.3.rs-467643/v1

Version of Record: A version of this preprint was published at Journal of Molecular Modeling on August 8th, 2021. See the published version at https://doi.org/10.1007/s00894-021-04862-6.

Abstract

The electronic, optical and vibrational properties of $B_3N_3H_6$ have been calculated by means of first-principles density functional theory (DFT) calculations within the generalized gradient approximation (GGA) and the local density approximation (LDA). The calculated structural parameters of $B_3N_3H_6$ are in good agreement with experimental work. With the band structure and density of states (DOS), we have analyzed the optical properties including the complex dielectric function, refractive index, absorption, conductivity, loss function and reflectivity. By the contrast, it is found that on the (001) component and (100) component have obvious optical anisotropy. Moreover, the vibrational properties have been obtained and analyzed.

1. Introduction

Borazine ($B_3N_3H_6$), which is generally introduced in textbooks as "inorganic benzene" under aspects of the isoelectronic relationship [1], is an ideal precursor for boron nitride materials because it only contains elements of boron, nitrogen and hydrogen [2]. It has been used as the precursor for preparation of both boron nitride ceramic matrix composites by PIP and boron nitride coatings by CVD [3]. Borazine was originally discovered by the thermal decomposition of the diammoniate of diborane [4]. Both experimental [5, 6] and theoretical [7, 8] works have been performed widely. The thermal decomposition of $B_3N_3H_6$ in unsaturated vapor has been studied [9], showing that the gaseous $B_3N_3H_6$ was decomposed on the reaction vessel surface along with the formation of volatile intermediates. The nature of chemical bond [10], ring current strengths [11], anion-π interactions [12] of $B_3N_3H_6$ were investigated, indicating its wide applications such as active molecule for electrodes [13], reactant for boron nitride nanowalls [14], low-dimensional spin filters [15, 16]. etc.

However, there are few studies in the literatures about physical properties of $B_3N_3H_6$. For example, the optical and vibrational properties associated with the material's structure are important to the military and civilian applications [17, 18], which have not been reported systematically. Therefore, our purpose is to calculate the electronic structure, optical and vibrational properties of $B_3N_3H_6$ by using the first-principles density functional theory.

2. Computational Details

The first-principles calculation with the Cambridge Sequential Total Energy Package (CASTEP) is employed in this paper [19]. LDA-CAPZ as well as GGA-PBE functional are applied as the exchange-correlation functional [20–23]. In order to consider the van der Waals interactions in $B_3N_3H_6$ crystal, the DFT-D methods is used, including the TS [24] and G [25] corrections. The pseudopotential is an effective potential constructed to replace the ionic core states, that is, the valence electrons are described by pseudo-wave functions [20–23]. For $B_3N_3H_6$, the ionic cores are represented by ultrasoft pseudopotentials. For B atom, the configuration is $1s^2 2s^2 2p^1$, where the $2s^2$ and $2p^1$ electrons are treated

as valence electrons; for N atom, the configuration is $1s^2 2s^2 2p^3$, where the $2s^2$ and $2p^3$ electrons are treated as valence electrons; for H atom, the configuration is $1s^1$, where $1s^1$ electron is treated as valence electron. The energy cutoff of 500 eV is applied in plane-wave basis. The Brillouin-zone integration is performed with 3×3×1 meshes using the Monkhorst-Pack method [26] for structure optimization. The values of the convergence thresholds for total energy, maximum force, maximum stress, maximum displacement are 5.0×10^{-6}eV/atom, 0.01eV/Å, 0.02 GPa and 5.0×10^{-4}Å.

3. Results And Discussion

3.1. Structural properties

The space group of tetragonal structure $B_3N_3H_6$ is $P4_32_12$. The crystal mode of $B_3N_3H_6$ is shown in Fig. 1 after structural optimization, it is an equilibrium crystal structure of Borazine. The optimized structural parameters of $B_3N_3H_6$ are given in Table 1 as well as experimental data. It can be seen that the values based on the GGA PBE-TS functional are in good agreement with the experimental results, indicating that this functional can well describe the crystal structure of Borazine. Hence, the physical properties of Borazine are solved by the GGA PBE-TS in the following work.

Table 1
The optimized structural parameters of $B_3N_3H_6$ along with the results of previous experimental data.

	This work			Experimental data [1]
	LDA	GGA PBE-G	GGA PBE-TS	
a (Å)	4.787	5.115	5.315	5.463
c (Å)	13.699	15.264	16.204	16.315

3.2. Electronic properties

The band structure of $B_3N_3H_6$ calculated within the GGA PBE-TS is shown in Fig. 2. From the band structure, it is shown that $B_3N_3H_6$ has an indirect band gap because the top of valence band is found at G point while the bottom of conduction band is found at A point. The band gap is calculated to be 5.007 eV, so we can know that $B_3N_3H_6$ is an insulator. The calculated band gap value is smaller than the experimental value of 6.5 eV [27]. The discrepancy is due to the well-known underestimation of DFT calculations. In the band structure, the valence bands are roughly divided into three regions: -16.0 eV to -14.0 eV (lower), -7.5 eV to 6.0 eV (middle) and − 4.5 eV to 0 eV (higher). Figure 3 shows the total and the partial density of states (DOS) of $B_3N_3H_6$. With the states between − 16 eV and − 12.5 eV, there is the interaction of N 2s, B 2p and H 1s. The states between − 8eV and − 5eV are predominantly composed of N

2p, B 2s and all hydrogen's 1s. The valence bands basically arise from interaction of N 2p, B 2p and H 1s states in the Fermi level.

3.3. Optical properties

The optical properties such as the complex dielectric function, complex refractive index, complex conductivity function, reflectivity, loss function and absorption coefficient are important, which can be obtained from the complex dielectric function [28]:

$$\varepsilon(\omega)=\varepsilon_1(\omega)+i\varepsilon_2(\omega) \quad (1)$$

In this section, we present our results of optical properties of $B_3N_3H_6$ at the equilibrium lattice constants in Figs. 4–9, up to a photon energy of 35 eV. We resolve the optical properties into two independent components: the polarization direction (001) component and the polarization direction (100) component. The calculated real part and imaginary part of complex dielectric function of $B_3N_3H_6$ are shown in Fig. 4. From this figure, the real part of complex dielectric function is $\varepsilon_{1\,(001)} = 2.209$ and $\varepsilon_{1\,(100)} = 2.298$. There is a peak ($\omega_{(001)} = 7.735$ eV, $\omega_{(100)} = 7.577$ eV) from 4.5eV to 9eV for imaginary part, which is attributed to transition from the valence bands to conduction bands (t_{2g}). There is a peak ($\omega_{(001)} = 13.225$ eV, $\omega_{(100)} = 12.863$ eV) for the calculated imaginary part, which is due to transition from the valence bands to conduction bands (e_g). The complex refractive index of $B_3N_3H_6$ is shown in Fig. 5. As shown in Fig. 5, we find that the static refractive index are $n_{(001)}(0) = 1.486$ and $n_{(100)}(0) = 1.516$. The refractive index reaches a peak at energy of 6.979 eV in (001) component, while it reaches a peak at energy of 6.806 eV in (100) component. Figures 6–9 show the absorption coefficient α(ω), complex conductivity function σ(ω), energy-loss function L(ω) and optical reflectivity R(ω). In each figure, as we can see, the optical anisotropy corresponds to the space group of $B_3N_3H_6$.

3.4. Vibrational properties

As shown in Fig. 10, there are 144 vibrations including 3 acoustic branches and 141 optical branches. The phonon spectra with no imaginary frequency reveal that $B_3N_3H_6$ is dynamically stable. There is no significant splitting, which indicates that the $B_3N_3H_6$ has no ability to change the strength of light as an optical device.

As shown in Fig. 10, the frequencies around 3450 cm^{-1} are referred to the vibrations of B-H and N-H, which are parallel to plane $(11\bar{1})$, $(\bar{1}\,\bar{1}1)$, $(1\,\bar{1}1)$ and $(\bar{1}11)$, including anti-symmetry and symmetry vibrations. It indicates that the B-H and N-H have a most dynamic strength. The frequencies around 2550 cm^{-1} are B-N anti-symmetric and symmetric vibrations, which are also parallel to above four planes. According to the calculated results, the vibrations of the frequencies above 896 cm^{-1} are parallel to four planes. The vibration of phonon is parallel to four planes at high frequencies, it shows that the crystal has a better dynamic stable when the optical radiation along those planes. Below 890 cm^{-1}, the

vibrations begin to be perpendicular and parallel to four planes as well as group vibration. It corresponds to a weak covalent bond strength, so the crystal has a low mechanical modulus and thermal conductivity.

4. Conclusions

We have investigated the structural, electronic, optical and vibrational properties of $B_3N_3H_6$. We found that the accurate equilibrium volume of $B_3N_3H_6$ from DFT calculations can be obtained by the TS correction to treat the van der Waals interactions. From the calculated band structure and density of states, we concluded that $B_3N_3H_6$ is an insulator with an indirect band gap of 5.007 eV. Moreover, the optical and vibrational properties of $B_3N_3H_6$ have been computed, indicating that there is an optical anisotropy and $B_3N_3H_6$ shows weak covalent bond strength.

Declarations

Acknowledgments Funding information is not applicable

Declaration of interests We declare that they have no known competing financial interests or personal relationships that could have appeared to influence the work reported in this paper.

Availability of data and material The data sets supporting the results of this work are included within the article, the other datasets generated during the current study are available from the corresponding author on reasonable request.

Code availability N/A

Authors' contributions Yun-Dan Gan: Writing - Original Draft, Investigation, Methodology, Data Curation. Han Qin: Methodology, Conceptualization. Fu-Sheng Liu: Theoretical analysis, Formal analysis. Zheng-Tang Liu: Visualization, Software, Supervision. Cheng-Lu Jiang: Formal analysis, Validation, Writing - Review & Editing. Qi-Jun Liu: Conceptualization□Writing - Review & Editing□Supervision.

References

1. Boese R, Maulitz AH, Stellberg P (1994) Chem Ber 127:1887
2. Lei MK, Ma TC (1996) J Inorg Mater 11:329
3. Li JS, Zhang CR, Li B (2011) Bulletin of the Chinese Ceramic Society 30:567
4. Wideman T, Sneddon LG (1995) Inorg Chem 34:1002
5. Chiavarino B, Crestoni ME, Marzio AD, Fornarini S, Rosi M (1999) J Am Chem Soc 121:11204
6. Islas R, Chamorro E, Robles J, Heine T, Santos JC, Merino G (2007) Struct Chem 18:833
7. Peyerimhoff SD, Buenker RJ (1970) Theoret Chim Acta 19:1
8. Kiran B, Phukan AK, Jemmis ED (2001) Inorg Chem 40:3615

9. Zavgorodnii AS, Timoshkin AYu (2018) Russian J General Chem 88:2476
10. Kalemos A (2018) Int J Quantum Chem 118:e25650
11. Rabanal-León WA, Tiznado W, Alvarez-Thon L (2019) Int J Quantum Chem 119:e25859
12. Bauzá A, Quiñonero D, Deyà PM, Frontera A (2012) Chem Phys Lett 530:145
13. Sen S (2017) Chem Phys 491:126
14. Merenkov IS, Kosinova ML, Maximovskii EA (2017) Nanotechnology 28:185602
15. Zhang CX, Guo H, Yang Z, Luo YH (2012) Acta Phys Sin 61:193601
16. Shao P, Ding LP, Luo DB, Lu C (2020) Molecular Phys 118:e1667542
17. Mammeri F, Bourhis EL, Rozes L, Sanchez C (2005) J Mater Chem 15:3787
18. Qin H, Zeng W, Liu FS, Gan YD, Tang B, Zhu SH, Liu QJ (2021) J Energ Mater 39:125
19. Clark SJ, Segall MD, Pickard CJ, Hasnip PJ, Probert MIJ, Refson K, Payne MC (2005) Z Kristallogr 220:567
20. Ceperley DM, Alder BJ (1980) Phys Rev Lett 45:566
21. Perdew JP, Zunger A (1981) Phys Rev B 23:5048
22. Perdew JP, Burke K, Ernzerhof M (1996) Phys Rev Lett 77:3865
23. Perdew JP, Chevary JA, Vosko SH, Jackson KA, Pederson MR, Singh DJ, Fiolhais C (1992) Phys Rev B 46:6671
24. Tkatchenko A, Scheffler M (2009) Phys Rev Lett 102:073005
25. Grimme S (2006) J Comput Chem 27:1787
26. Monkhorst HJ, Pack JD (1976) Phys Rev B 13:5188
27. Zunger A (1974) J Phys C: Solid State Phys 7:76
28. Gao J, Zeng W, Tang B, Zhong M, Liu QJ (2021) Mater Sci Semicond Process 121:105447

Figures

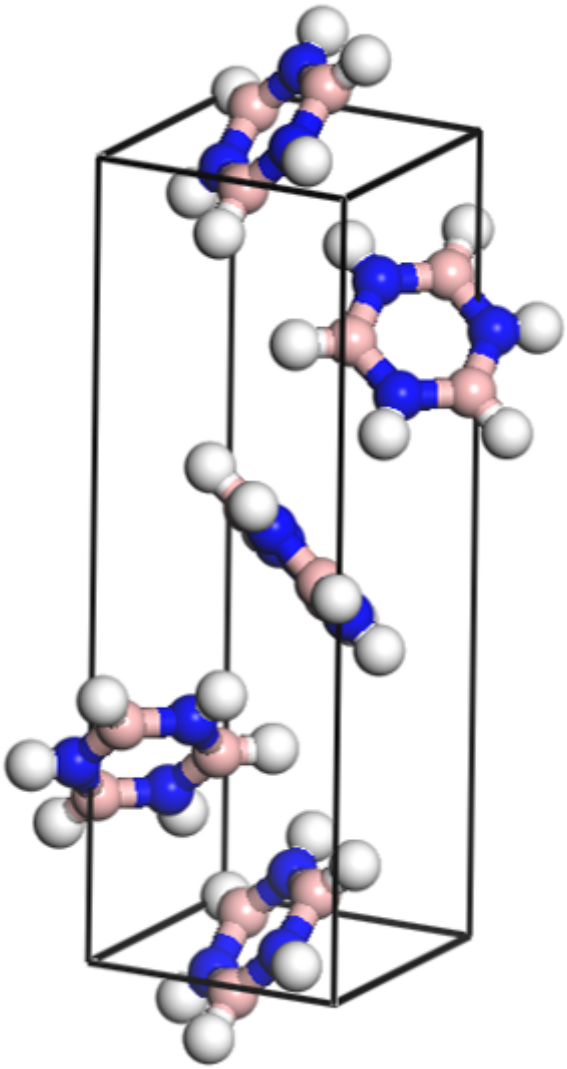

Figure 1

The crystal structure of B3N3H6 (B atoms are pink, N atoms are blue and H atoms are white).

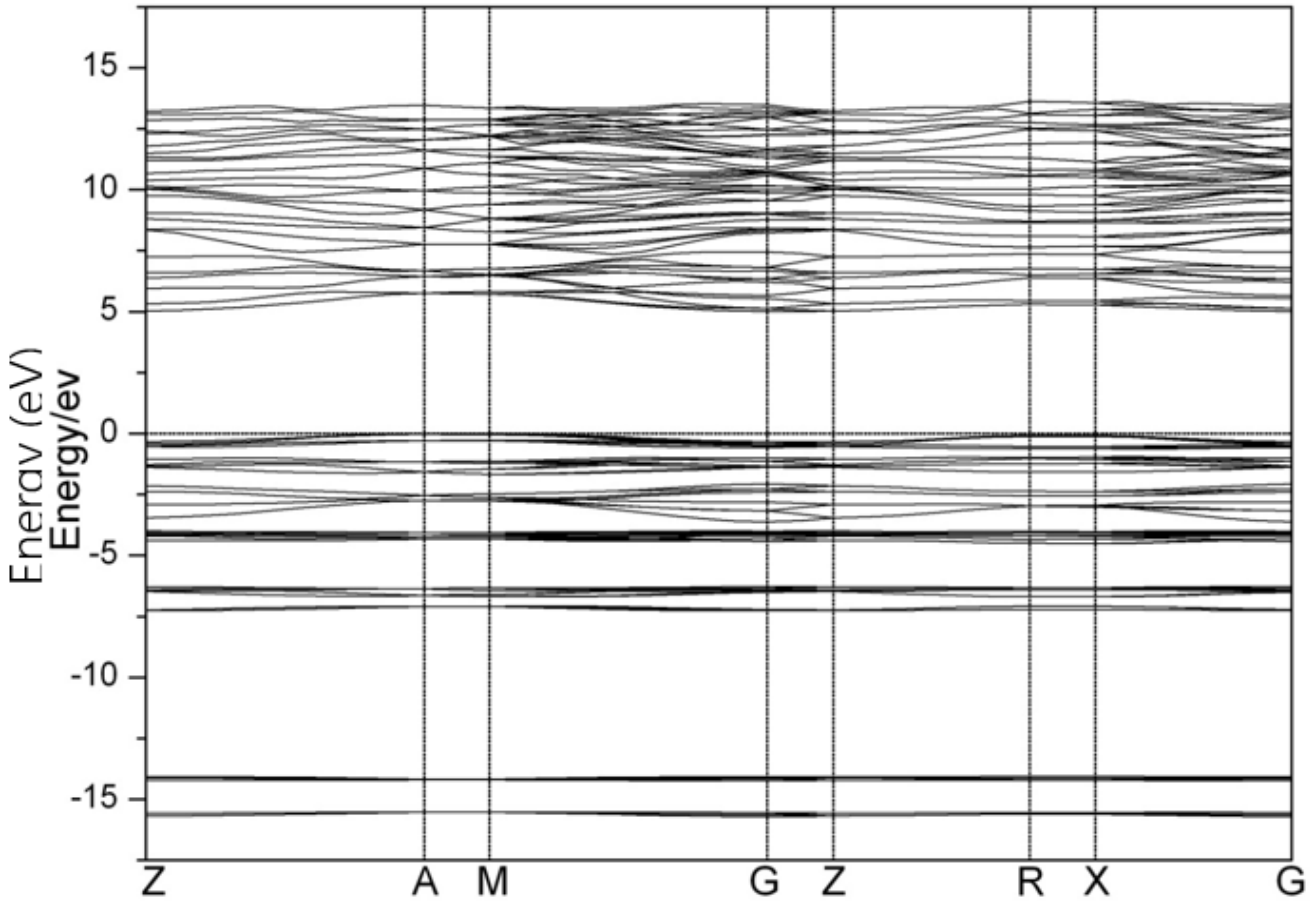

Figure 2

The band structure of B3N3H6 from the GGA PBE-TS calculation

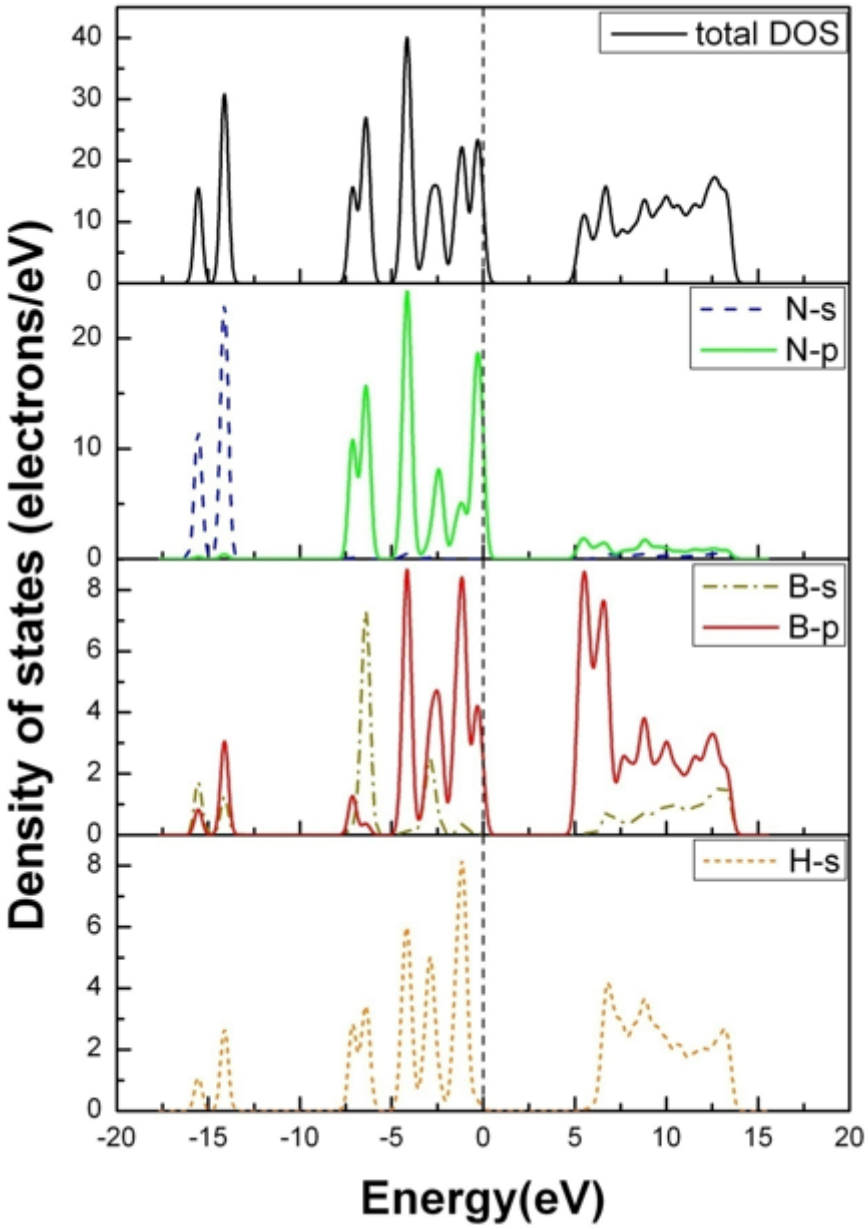

Figure 3

The density of states of B3N3H6 from the GGA PBE-TS calculation

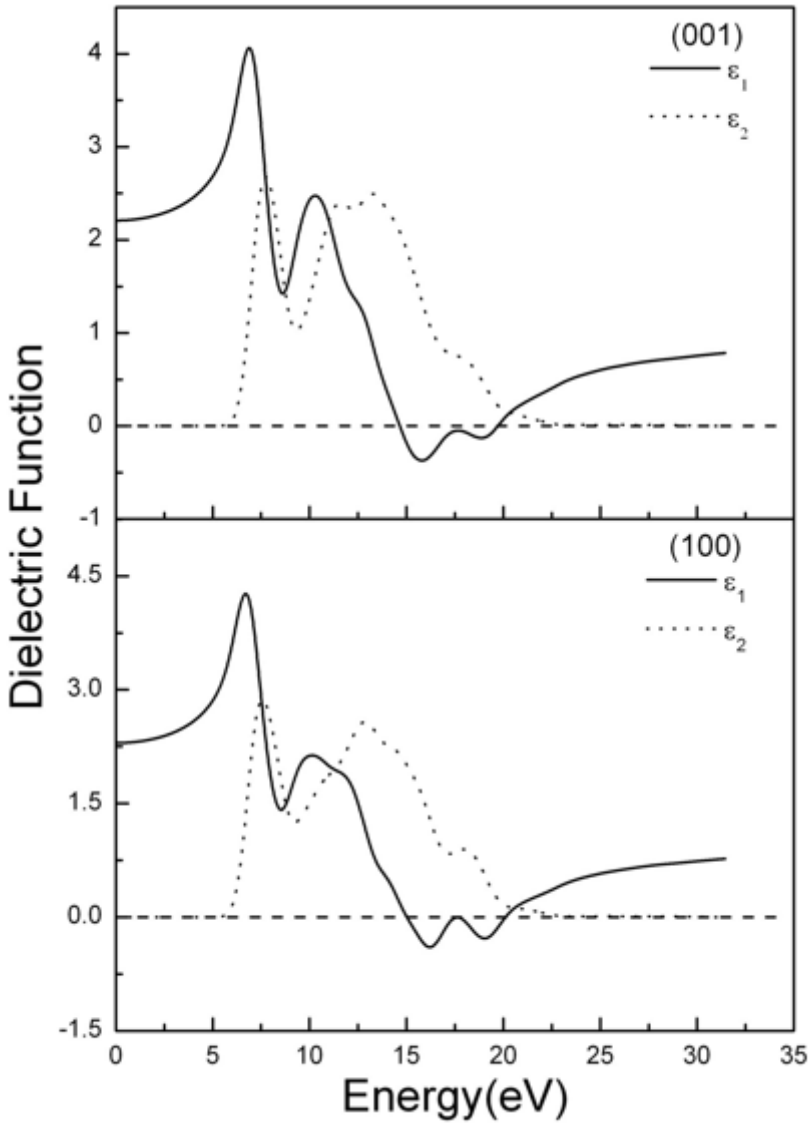

Figure 4

The real and imaginary part of dielectric function of B3N3H6 for polarization direction (001) and (100)

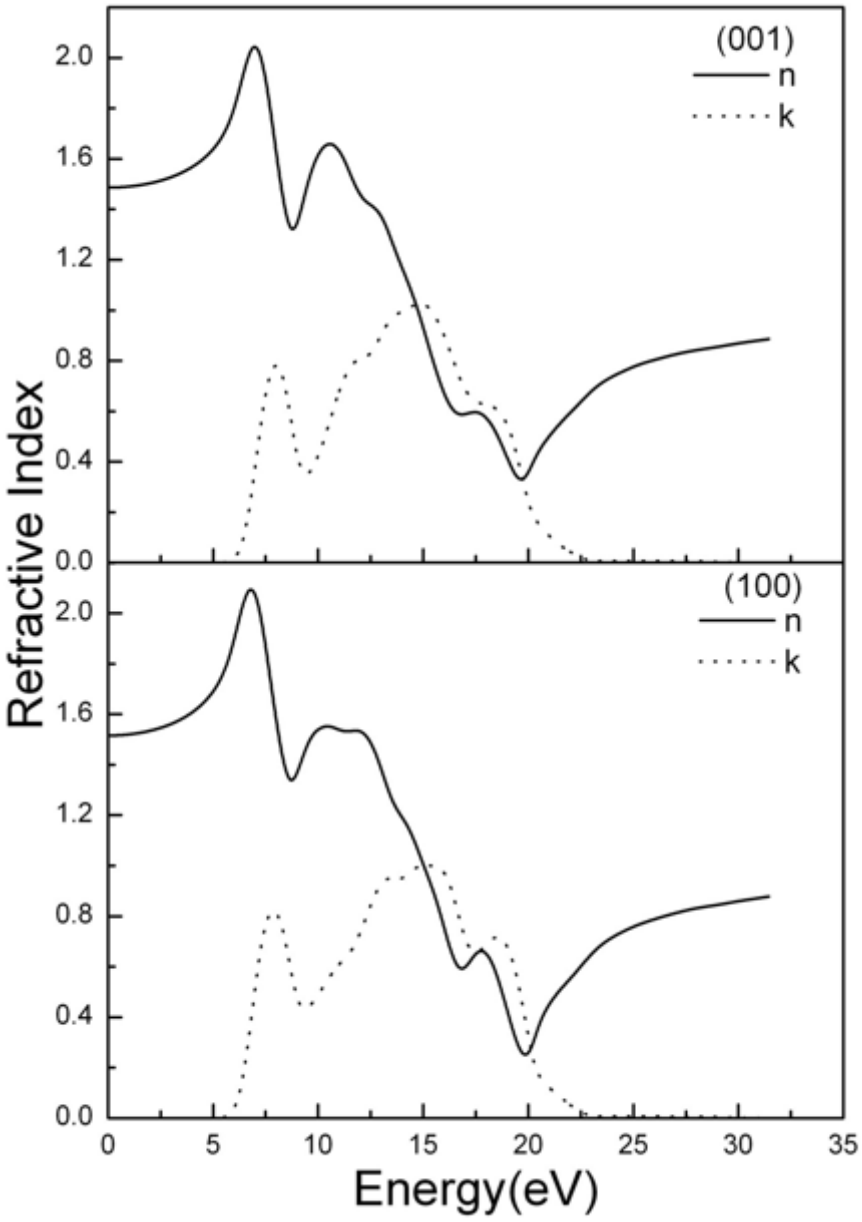

Figure 5

The real and imaginary part of refractive index of B3N3H6 for polarization direction (001) and (100)

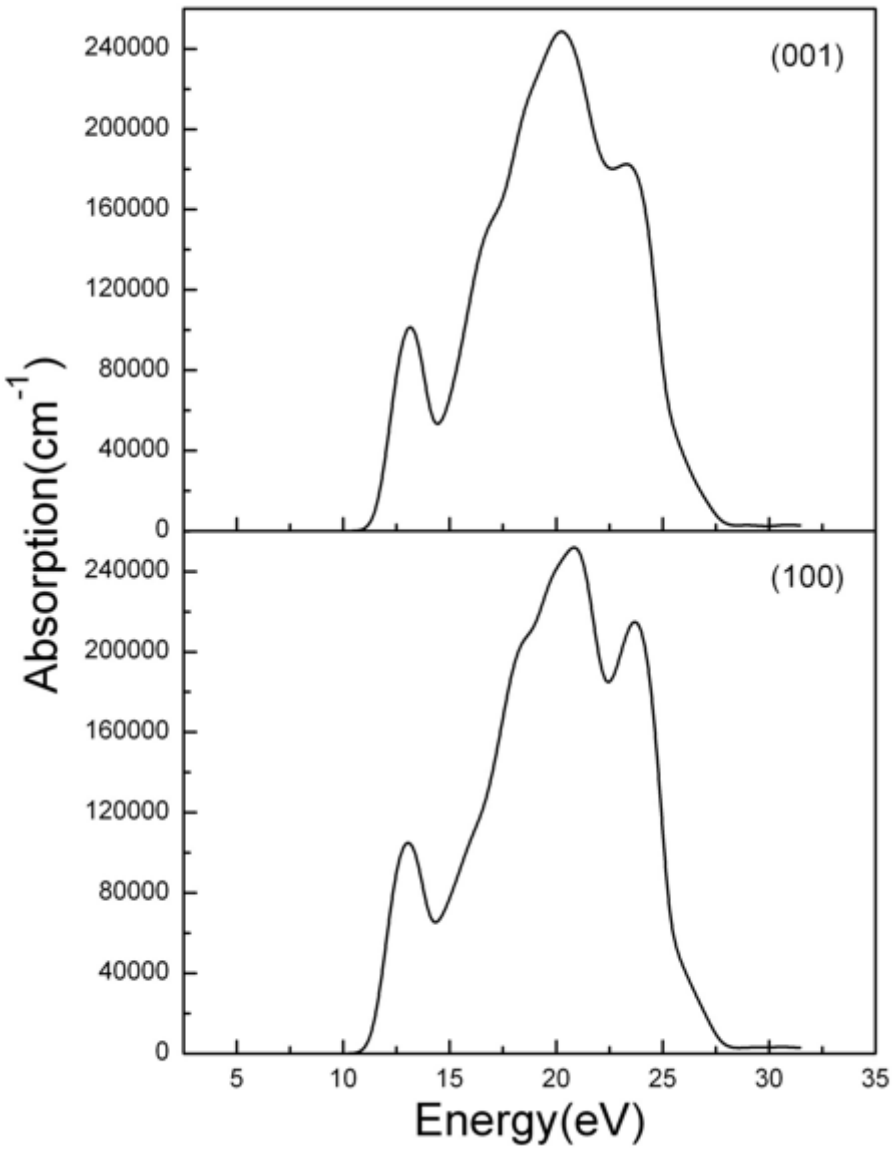

Figure 6

The absorption coefficient of B3N3H6 for polarization direction (001) and (100)

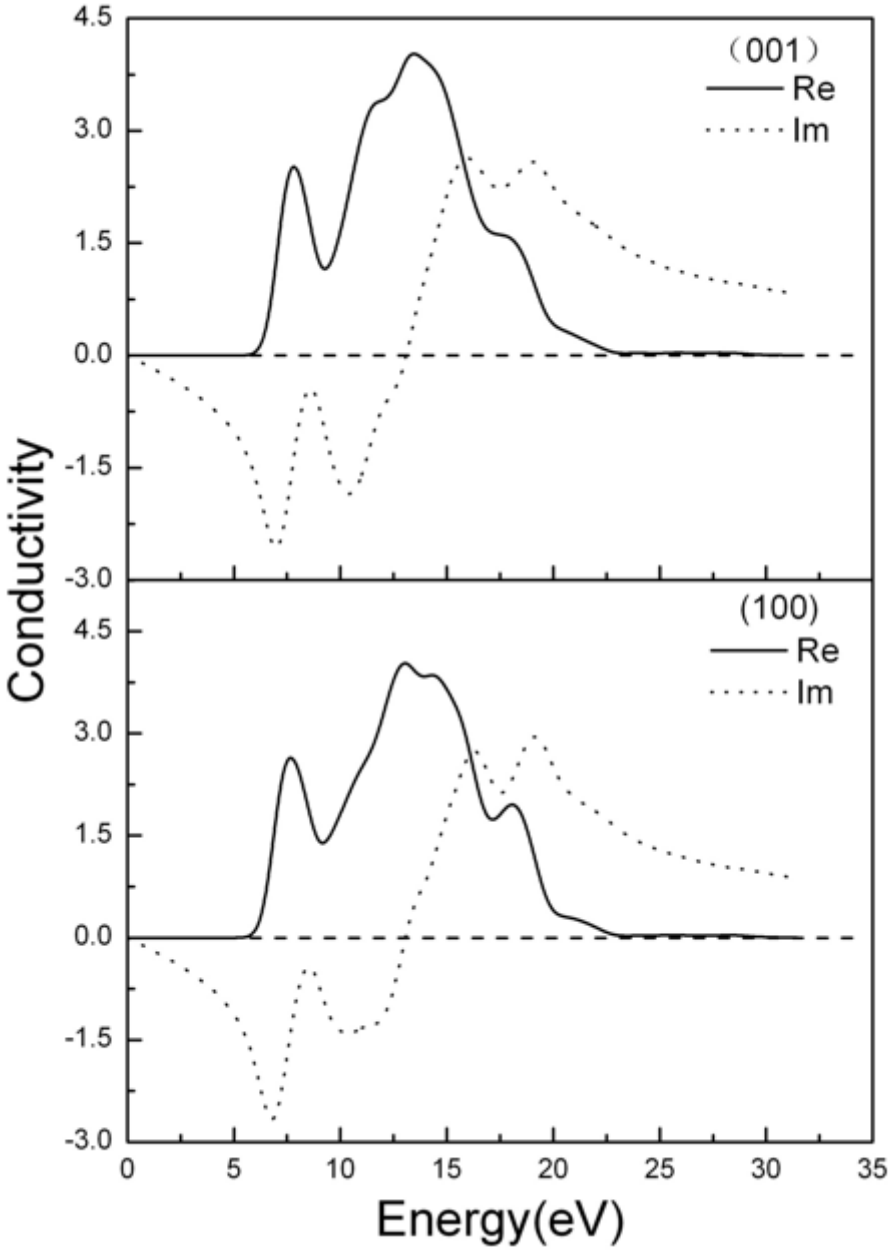

Figure 7

The complex conductivity of B3N3H6 for polarization direction (001) and (100)

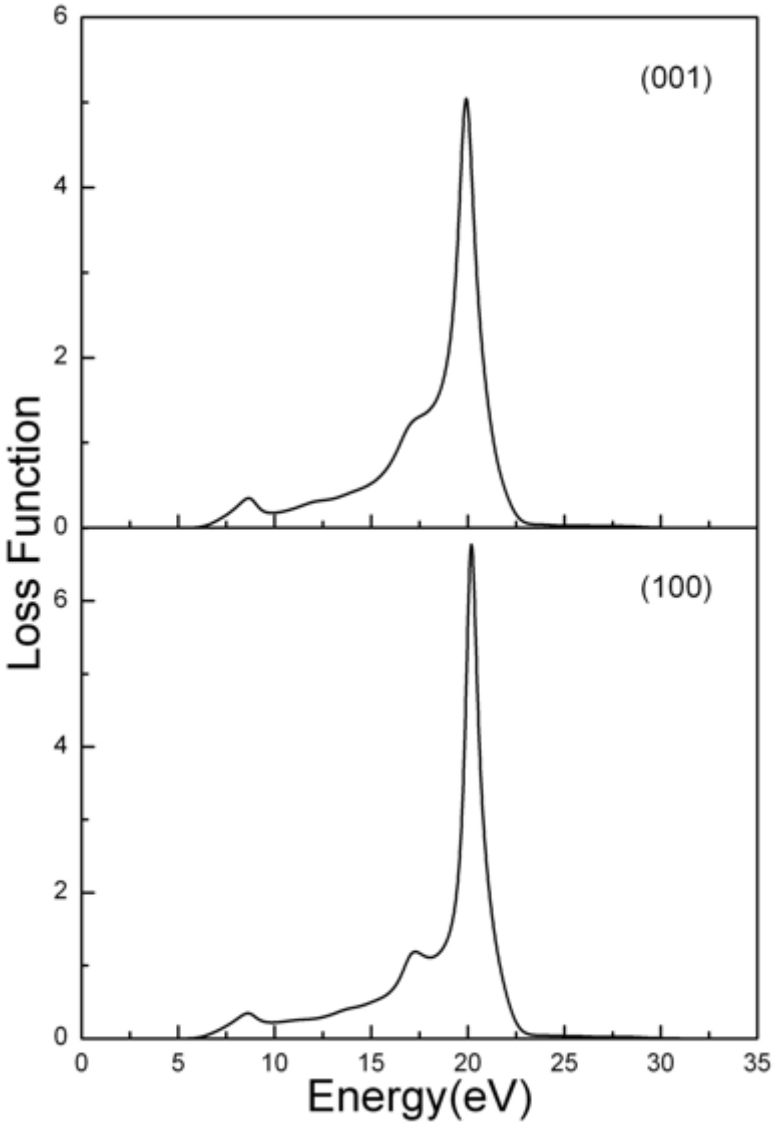

Figure 8

The energy-loss function of B3N3H6 for polarization direction (001) and (100)

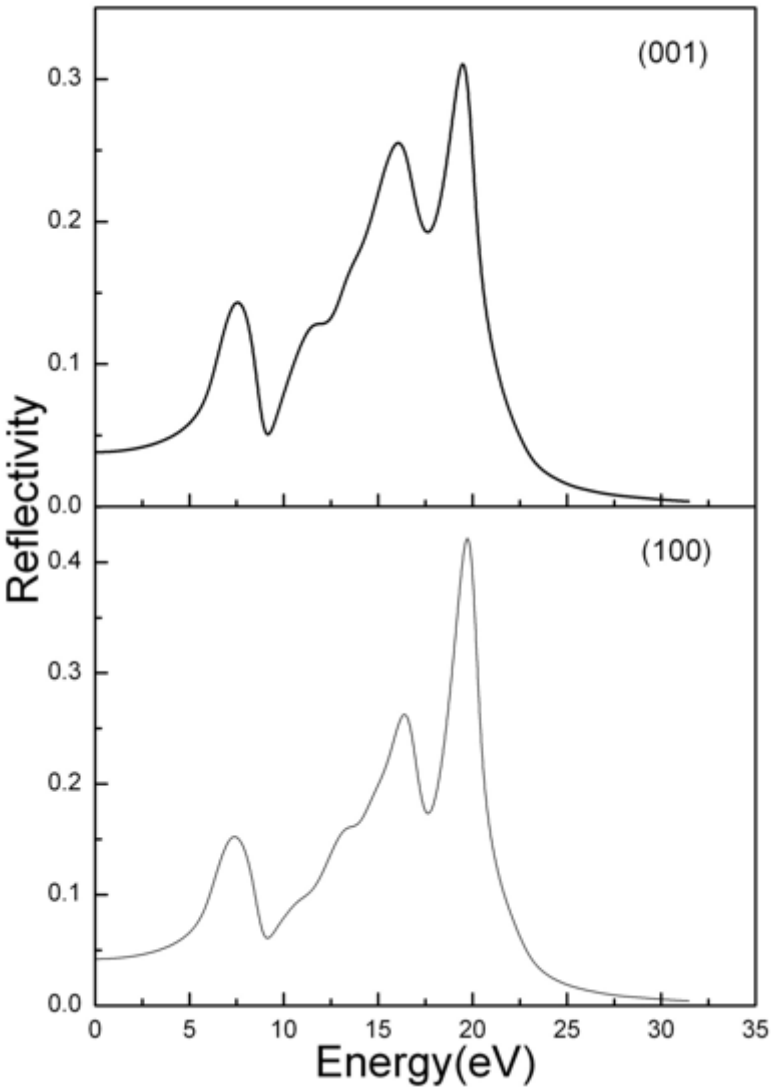

Figure 9

The optical reflectivity of B3N3H6 for polarization direction (001) and (100)

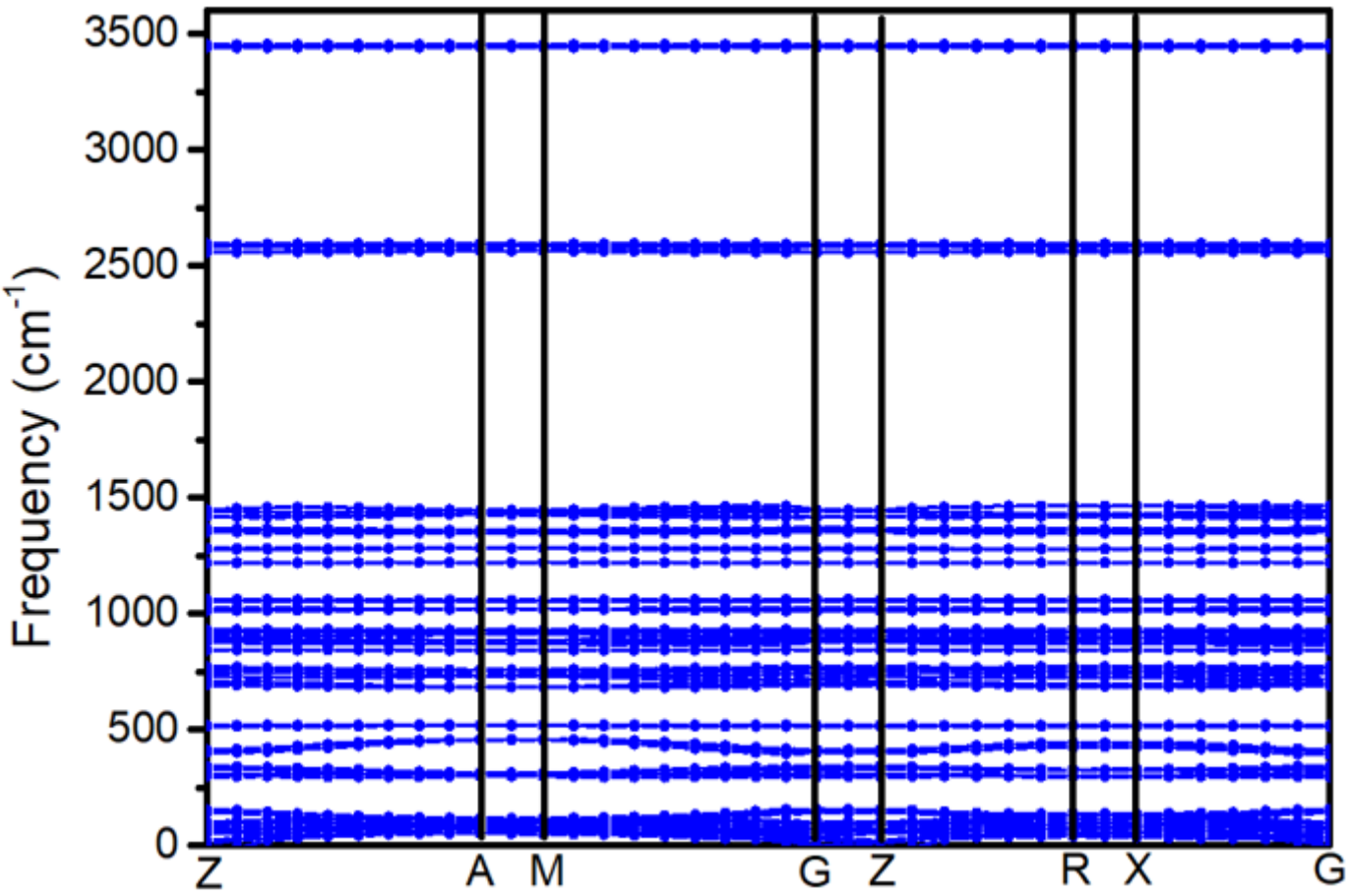

Figure 10

Calculated phonon dispersion of B3N3H6